2021

Effect of high energy ball milling on spherical metallic powder particulates for additive manufacturing

Ansell, Troy Y.; Hanneman, Timothy; Gonzalez-Perez, Andres; Park, Chanman; Nieto, Andy

Taylor & Francis

Ansell, Troy Y., et al. "Effect of high energy ball milling on spherical metallic powder particulates for additive manufacturing." Particulate Science and Technology (2021): 1-9.

http://hdl.handle.net/10945/67202

PARTICULATE SCIENCE AND TECHNOLOGY
https://doi.org/10.1080/02726351.2021.1876192

Taylor & Francis
Taylor & Francis Group

Effect of high energy ball milling on spherical metallic powder particulates for additive manufacturing

Troy Y. Ansell, Timothy Hanneman, Andres Gonzalez-Perez, Chanman Park, and Andy Nieto

Department of Mechanical and Aerospace Engineering, Naval Postgraduate School, Monterey, California, USA

ABSTRACT

Properties, such as morphology, particle size, and hardness affect the ability of a powder to flow and bond to a surface in additive manufacturing (AM) applications. The effects of high energy ball milling on spherical copper and stainless steel powders were evaluated. Morphology of both stainless steel and copper powders, quantifiable by aspect ratio, showed larger changes due to ball-to-powder ratio (BPR, 2:1–1:10) compared to the total milling time (2–60 min). Hardness of copper increased from 53 $HV_{0.01}$ in the as-received condition to 96 $HV_{0.01}$ after milling for 60 min with a BPR of 1:1 or 2:1. Hardness of steel increased from 336 $HV_{0.01}$ in the as-received condition to 523 HV0.01 after milling for 60 min with a BPR of 2:1. Hardness of both powders was insensitive to milling times at low BPR (1:10). At high BPR (2:1), hardness of steel increases after just 2 min of milling, while Cu changed significantly only after 60 min. Hardness was influenced more by BPR than by milling time. It is shown that a broad range of milling parameters exist where metallic powders can be processed with minimal changes to their morphology, while controlling for hardness.

KEYWORDS

Cold spray; additive manufacturing; high energy ball milling; steel powder; copper powder

1. Introduction

Metal powders are used in additive manufacturing (AM) techniques such as laser bed metal fusion and cold gas dynamic spray. Laser bed metal fusion is a term broadly used for any AM metal process where a part is built up layer wise by a laser which melts, or sinters, metal powder spread out in a bed, for example, selective laser melting (SLM) (Frazier 2014). Cold gas dynamic spray, or cold spray, is another AM technique used for adding a coating layer to a substrate or building a complete part in a layer wise fashion (Li et al. 2018; Raoelison et al. 2018). In cold spray, feedstock metal powder passes through a convergent–divergent nozzle, also known as a de Laval nozzle. The powder is accelerated by a high-pressure gas reaching high velocities with sufficient kinetic energy to adhere to a substrate. In both processes and in other similar techniques, powder flowability affects the coating layer density and thickness among other properties. In SLM, poor flowability leads to a non-continuous bed of powder that directly translates into porosity in the final part. Powder flowability is effected by particle properties including morphology of the particles and the particle size distribution (Spierings et al. 2016). Powder characteristics can be engineered for these manufacturing processes by several methods. Changing size and morphology of particles contained within a powder can be accomplished by mechanical milling techniques, such as high-energy ball milling (HEBM). HEBM is suited for powder morphology modification, grain size refinement, reactive milling, and incorporation of secondary phases into composite powder feedstocks.

HEBM (also known as mechanical alloying) was originally developed to combine the benefits of high-temperature oxide dispersion hardening with lower temperature precipitation hardening in nickel alloys for use in gas turbine engines (Gilman and Benjamin 1983). The technique is a dry process, that is, no liquids or surfactants are used during milling. Particles are subjected to repeated collisions with milling media leading to cycles of interparticle welding and fracturing (Gilman and Benjamin 1983; Suryanarayana 2001). Since the technique's inception in the late 1960s, the use of HEBM has expanded to producing powders of intermetallic alloys (Gilman and Benjamin 1983; Wolski et al. 1996; Chen, Hampikian, and Thadhani 1999); the study of mechanically induced crystallization of amorphous metal alloy powders (Trudeau et al. 1990); reducing the size of ceramic particles to the nano regime for use as a catalyst in chemical processing (Ayoman and Ghorban Hosseini 2016) or in carbon monoxide sensors (Ghasdi and Alamdari 2010); and the production of fine ceramic powders made of lead zirconate titanate for use in piezoelectrics (Kong, Zhu, and Tan 2000). Composite powders have been synthesized with HEBM. Through ball milling, aluminum powders were reinforced with nanodiamond (ND) powders resulting in improved hardness and wear resistance after consolidation

CONTACT Troy Y. Ansell troy.ansell@nps.edu; Andy Nieto andy.nieto@nps.edu Department of Mechanical and Aerospace Engineering, Naval Postgraduate School, Watkins Hall, 700 Dyer Rd., Monterey, CA, USA.

(Kaftelen and Öveçoğlu 2012). Stainless steel 316L was found to exhibit course particles with fine grain structure after HEBM (Zheng et al. 2016) indicating control of particle microstructure and powder properties.

HEBM parameters like ball-to-powder ratio (BPR) or milling time affects the underlying particle properties. Woo et al. performed research on ND–Al metal matrix composites, investigating the role of BPR on the resultant properties, such as hardness. As BPR increased, hardness increased if milling times were less than 2 h (Woo et al. 2013). Heat-resistant 300 type stainless steel scrap was processed by HEBM into nanosized particles. The stainless steel nanoparticles exhibited a transition from austenite to martensite leading to increases in hardness. The percentage of martensite depended on the milling time of the powders. Longer milling times led to higher martensite content, which subsequently resulted in higher hardness (Enayati, Bafandeh, and Nosohian 2007). Mechanical alloying conditions were tested on nanoparticles of copper. Boytsov et al. found that copper nanoparticle properties were dictated by energy of collisions (Boytsov et al. 2007). Milling speed was found to decrease crystallite size of copper particles during mechanical alloying of copper particles with NbC particles (Zuhailawati, Salihin, and Mahani 2010).

AM techniques, like SLM and cold spray, require precise control of powder properties to ensure reproducible and reliable 3D-printed parts and material. To the authors' knowledge, there has been no systematic study of the effect of ball milling parameters on powder properties like morphology and hardness, especially under relatively low energy conditions. In this article, an investigation of the effects of adjusting ball milling conditions to precisely control powder morphology and subsequent hardening is conducted. The parameters BPR and cycling times were adjusted and the resulting changes to powder morphology and hardness of stainless steel and copper powders were studied. This study provides a parameter space for researchers and engineers to be able to mill spherical powders without significantly altering their shape, which would adversely affect their flowability in AM applications.

2. Materials and methods

2.1. Powder processing

Two commercially pure cold spray powders were used: Cu powder (ACuPowder International, LLC, Union, NJ) and 316L Stainless steel powder (SST-5002 Centerline Windsor LTD., Windsor, Canada) to investigate a soft and medium hardness metal. High hardness metals are not currently common in many AM applications. In each milling run, a high-energy ball mill (HEBM, SPEX Sample Prep Mixer/Mill 8000 D) was used with 40 g of powder, and steel balls weighing approximately 1.0 g each. Multiple BPRs were investigated: 2:1, 1:1, 1:5, and 1:10. The HEBM was run for 2 min on and left to "cool" for 5 min off to complete one cycle. As such, once cycle represents 2 min of actually milling. A total of 40 samples were processed in batches of one, two, five, ten, and thirty cycles, corresponding to milling times of 2−60 min. As-received powders served as experimental controls.

For the rest of this article, the following naming scheme will be used to identify samples. As-received stainless steel and copper will be referred to as SS and Cu, respectively. The processed powders will be named with the composition followed by the BPR and the number of cycles separated by a dash. For example, copper powder milled at a 1:10 ratio for 10 cycles is Cu-1:10-10.

2.2. Materials characterization

Milled powders were cold mounted using a Struers Epofix resin/hardener. The mounted samples were polished with a Buehler Ecomet 3 variable speed grinder for varying grit up to p2500 (1200 grit). These samples were then imaged with a Nikon Epiphot 200 microscope for transversal cross-sectional examination. Hardness testing was conducted using a Struers DuraScan 50 with a HV setting of 0.01. Metal powders were also spread on carbon tape and prepared for imaging with a Zeiss Neon 40 scanning electron microscope (SEM). Electron imaging was performed with an Everhart-Thornley secondary electron detector set to 2 kV accelerating voltage, a 30 μm objective aperture, and working distances between 5.0 and 10 μm. To measure the aspect ratio of the particles, images were processed and analyzed with ImageJ (National Institutes of Health). Images were first processed into a binary color format and then analyzed with the analyze particle feature. The elliptical measurement tool was used. Particles on the edge were excluded. A minimum particle size of 5.0 μm was used for the copper samples. Lower size limit for SS specimens was 6.0 μm and the upper limit was 2500 μm except for samples with larger particles (e.g., powders processed at 2:1 or 1:1 and 30 cycles) which required an upper limit of 10,000 μm. The elliptical shapes were compared to the original image and false positives were manually removed.

3. Results and discussion

3.1. Evolution of powder morphology

3.1.1. Starting powder characteristics

Seen in Figure 1(a) are SS powders and in Figure 1(b), Cu powders. The SS powders had two general groups of particles: the prevalent group consists of large, similar-sized particles and the second group consists of a relatively minor fraction of finer particles. This variation in particle accounts for the wide standard deviation seen in the starting powder and subsequent HEBM processing powder. While the particulates are largely spherical, it is acknowledged that a few irregular particulates exist. What appear as joined or elongated particulates can result from the atomization process or heat treatments thereafter. In Figure 1(b), Cu powders can be seen to be smaller as compared to the SS powders. These powders similarly had a wide distribution of sizes, mostly large regular sized particulates with a few finer particulates. Finer particulates were not sieved out as it was desirable to see how they would interact with larger particulates during

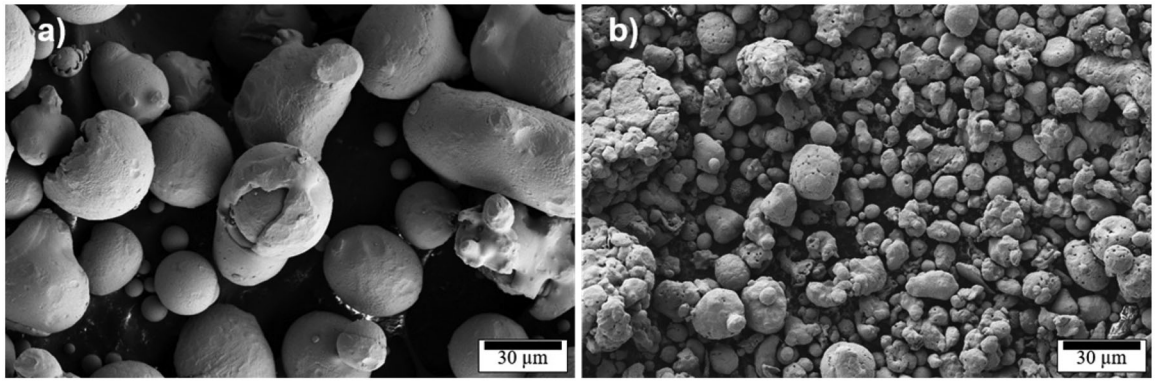

Figure 1. SEM images of as received: (a) SS powders and (b) Cu powders.

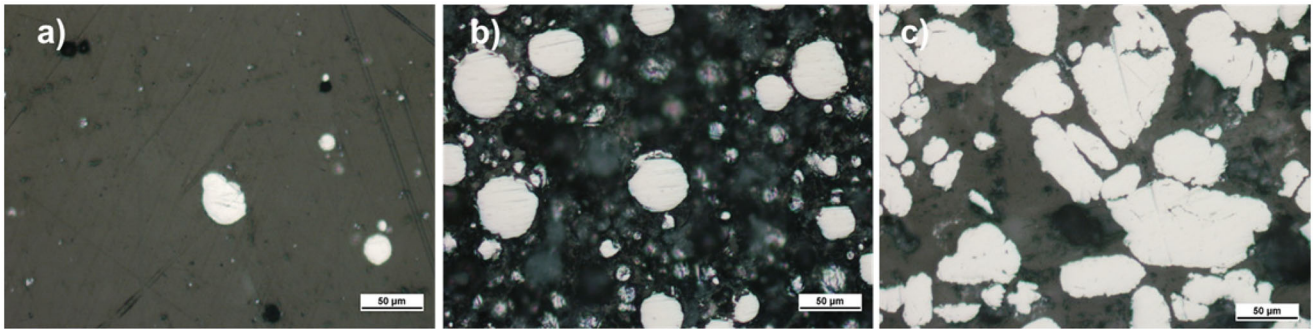

Figure 2. Optical micrographs (scale: 50 µm) of as-received and milled powder cross-sections, (a) as-received SS powder, (b) SS-1:10-2 powders, and (c) SS-2:1-30 powders.

HEBM. In the Cu powder, agglomerates were occasionally found.

3.1.2. Morphology and aspect ratio of stainless steel powders

Figure 2(a) shows cross-sections of the stainless steel powder. Stainless steel powder milled at a 1:10 ratio for 2 cycles are shown in Figure 2(b). Changes are minimal and powder retains spherical shape very well. Smaller particulates remain independent and separated from larger particulates. SS-2:1-30 powders are shown in Figure 2(c) and what is observed is a flattening of particles leading to an increase in the aspect ratio. In addition, the presence of smaller particulates is nearly non-existent. Instead, a close look at the particulate surface reveals that smaller elongated particulates appear on the surface, and in some cases small clusters of small, elongated particulates are seen. A BPR of 2:1 represents a high energy milling condition and as such impact force is great enough to deform the smallest particulates first. Additionally, high momentum of larger particulates will effectively make them milling media relative to smaller particulates. Particulate flattening is due to the higher milling energy and prolonged milling time that leads to the momentum and number of collisions increasing, respectively. Aspect ratio generally increased with longer and higher energy processing of SS powders, however, higher energy (higher BPR) had greater influence.

Figure 3 shows a series of SEM images of SS samples milled with various parameters. The top row is micrographs of 1:10 milled SS powders cycled 2, 10, or 30 times. Images in the middle row are samples milled with at a BPR of 1:1 for 2, 10, or 30 cycles and the bottom row is 2:1 samples milled 2, 10, or 30 times. What was observed in Figure 3 confirms observations found in Figures 2(a–c), increasing the mass of milling media to powder mass and increasing the number of cycles flattens the particles. Powders milled at a 1:10 ratio exhibited relatively low changes in morphology with increasing number of cycles. Compare SS-1:10 samples with SS-1:1 and SS-2:1 respectively and was observed is a reduction in the number of cycles needed for an increase in aspect ratio. When the milling ratio is close to 1:1 and the number of cycles exceeds 10, powders will see a change in morphology and an increase in aspect ratio. Generally, the occurrence of flake-like particulates is uncommon in the conditions examined and the spherical morphology is largely preserved. This is evidenced by the gradual changes in aspect ratio measured.

Aspect ratio for SS powders is quantified and plotted in Figure 4. Seen are plots of the measured aspect ratios (vertical axis) *versus* number of cycles (horizontal) for all samples both milled and unmilled. The plots are arranged such as the relatively mass of the powders decreases from the top of the figure. Result for unmilled powder is labeled SS and is the same for all plots. For all milling ratios, the aspect ratio gradually increased to 2.0 as the number of cycles increased. For higher and consistent aspect ratio in stainless steel powders, the milling ratio should be at minimum 1:1 and the number of cycles should be higher than 10.

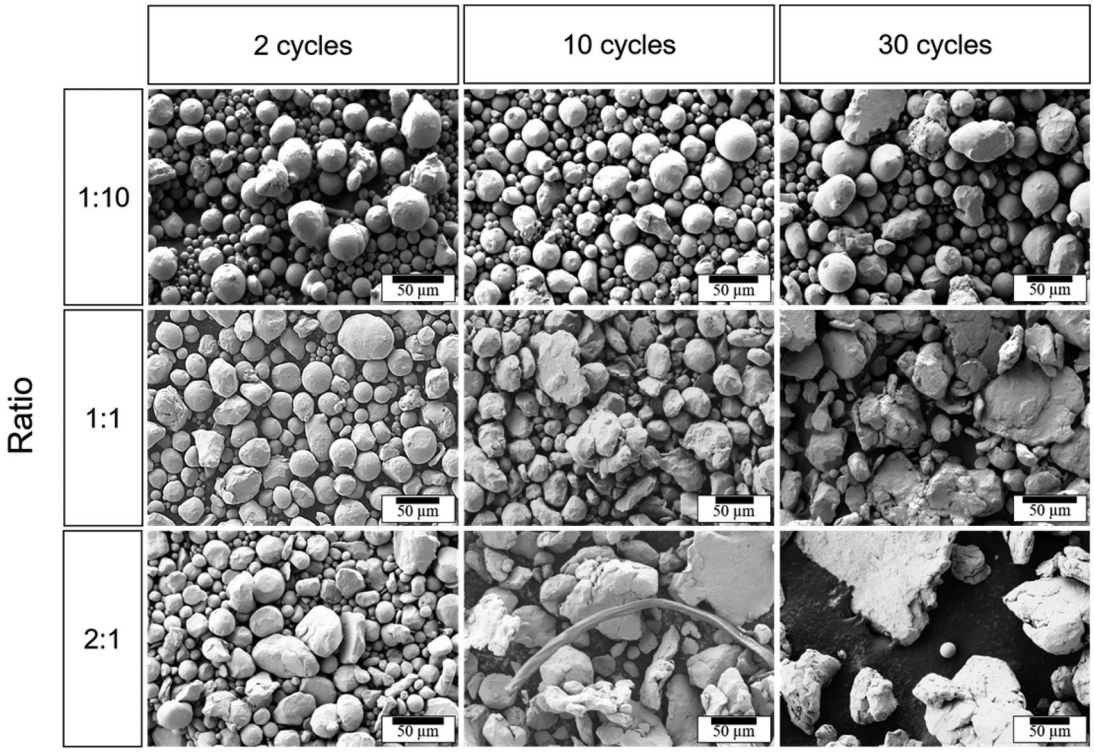

Figure 3. SEM images of milled 316L stainless steel powders processed at different BPRs and under varying cycles.

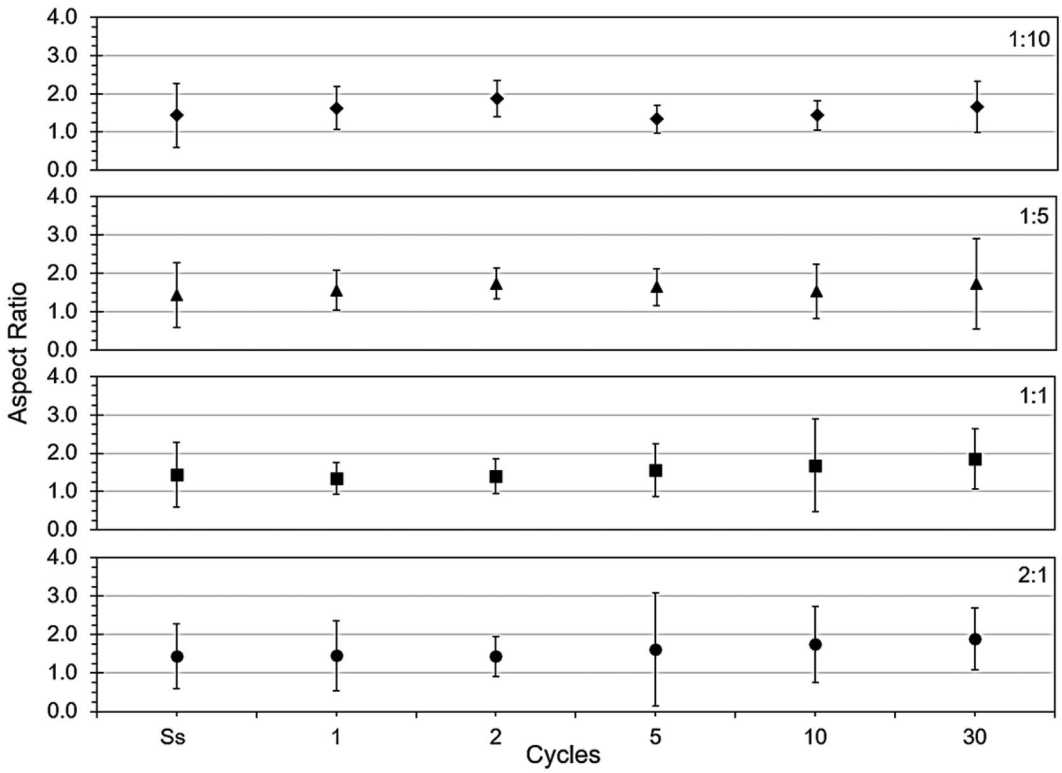

Figure 4. SEM images of milled 315L stainless steel powders processed at different BPRs and under varying cycles.

3.1.3. Morphology and aspect ratio of copper powders

Optical images of cross-sectioned Cu particles are shown in Figure 5(a–c). Aside from being finer than SS, these particulates exhibit more deviations in spheroidicity. The prevalence of smaller particulates may in part account for the presence of agglomerates in the as-received Cu power. Cu-1:10-2 and Cu-2:1-30 powders are shown in Figures 2(b,c), respectively. As with the SS powders, increasing the mass of milling media relative to the powder mass (increasing milling energy) and increasing the number of milling cycles (increased milling time and number of collisions) caused flattening of individual particles. It was noted that

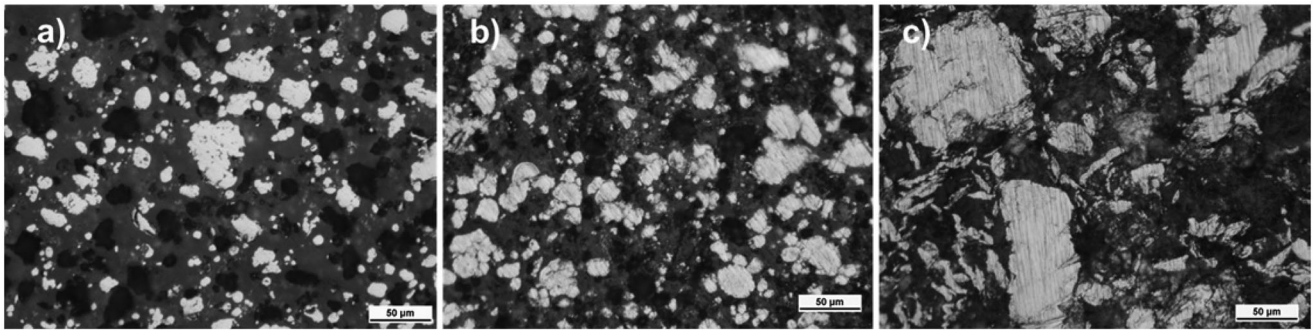

Figure 5. Optical micrographs of cross-section copper powders (scale bar: 50 µm), (a) As-received Cu; (b) Cu-1:10-2; and (c) Cu-2:1-30 powders.

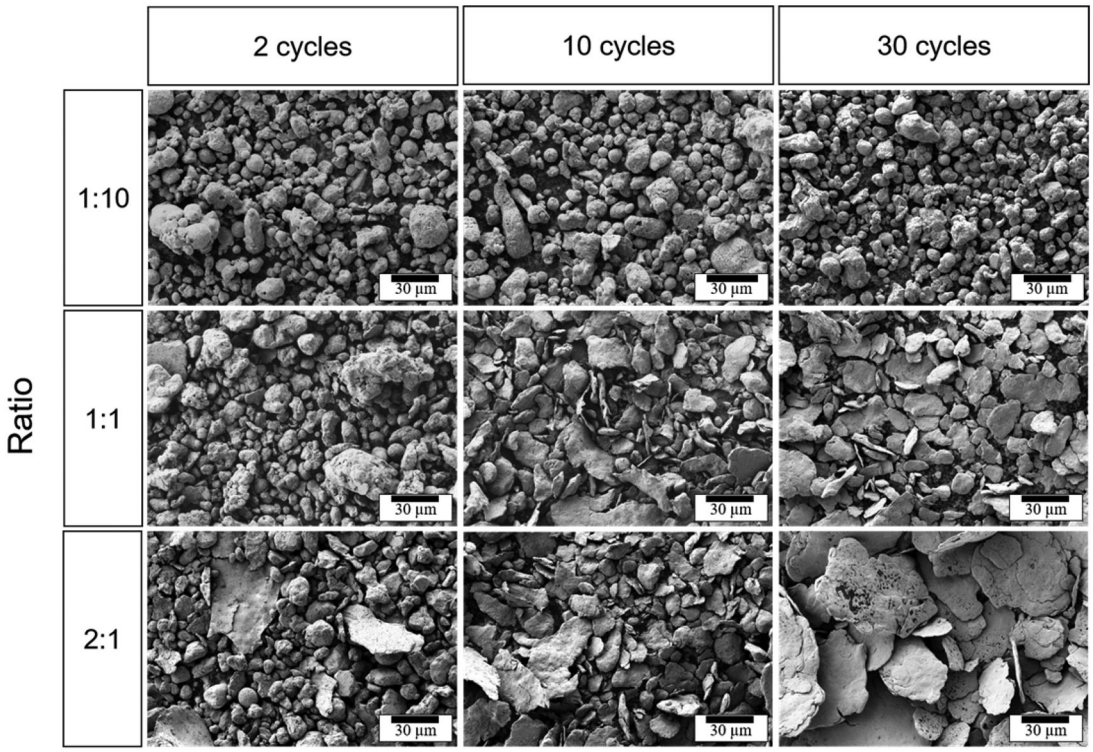

Figure 6. SEM images of milled copper powders processed at different BPRs and under varying cycles.

Cu powder milled at a 2:1 ratio for 30 cycles had a significant portion of agglomerates, resulting in an overall increase in particulate size. These larger particulates are made of smaller particulates that have flattened onto each other and may have welded together. Welding during both low and HEBM is well-known (Witkin and Lavernia 2006) and the lack of porosity within the larger particulates supports this observation. The occurrence of small spherical particulates is absent, instead many small high aspect ratio flakes are seen.

Figures 6 and 7 show the changes in morphology and quantification of aspect ratio changes in processed Cu powders. Figure 6 is arranged in the same way as Figure 3 with number of cycles increasing to the right and relative ball milling media mass increasing from top to bottom of the image. A one-to-one ratio after 10 cycles was enough to flatten a significant number of particles as seen in the center image. "Larger flakes plates" of copper were seen to be forming after two cycles when the ratio was 2:1. The largest flakes of copper were seen at a 2:1 ratio and after 30 cycles as seen in the lower right-hand corner image. The aspect ratio was highest after milling at a 2:1 ratio for 30 cycles. As with SS, the aspect ratio of Cu powders increased with an increase in relative milling media mass and an increase in the number of milling cycles. However, the relative softness of Cu compared with the steel milling media led to much greater loss of spheroidicity and formation of Cu flakes. Measured aspect ratios and microhardness values for as received and HEBM processed powders are tabulated in Table 1.

The aspect ratios of Cu samples, seen in Figure 7, increases from 1.7 to a maximum of 2.4 for the Cu-1:1-10 sample. Of note is the increase in variance of aspect ratio with an increase in the relative milling media mass. Although the flakes or possible agglomerates increase in size with milling cycle and ratio, the distribution of sizes of the flakes also increases. It should be noted that the algorithm used to calculate aspect ratio was designed to measure spheriodicity and measured a major and minor axis only.

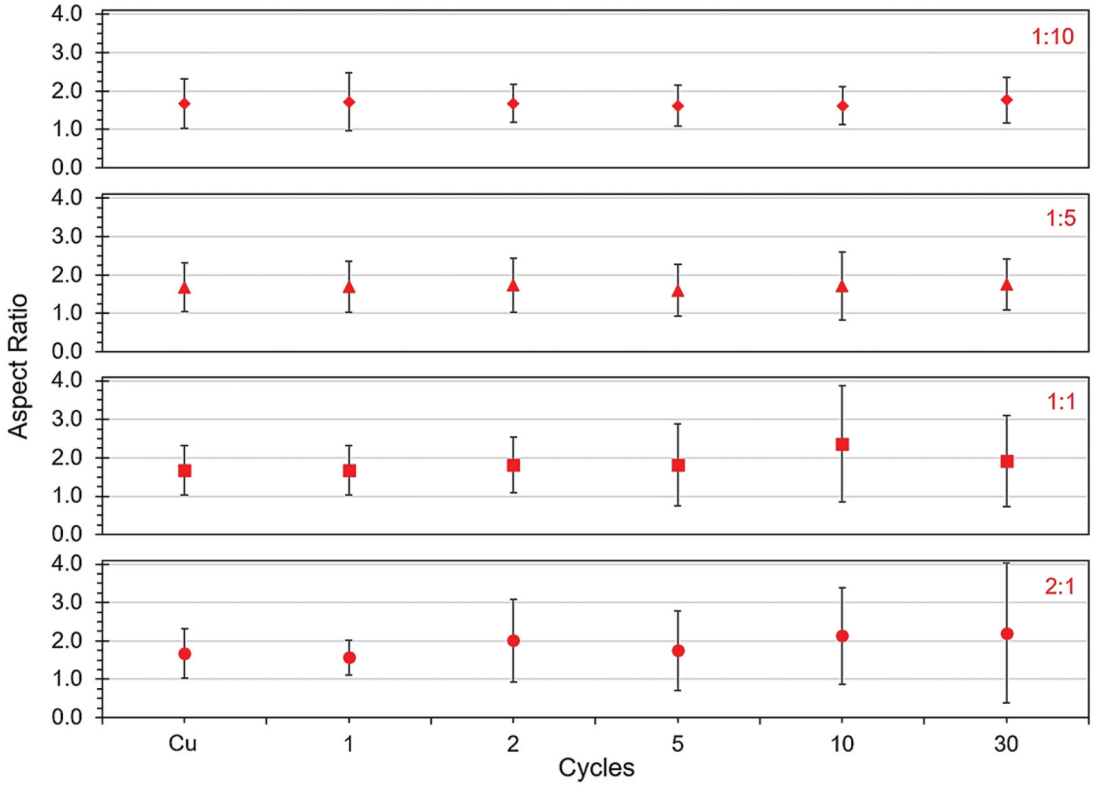

Figure 7. SEM images of milled 316L stainless steel powders processed at different BPRs and under varying cycles.

No measurements of the thickness could place, and as such the flake morphology was not quantified. However, SEM images show a few flakes in-plane, and it can be seen that there thickness is no more than a micron, while the lateral dimensions are often well over 30 um, which would results in a flake aspect ratio of >30. While not quantified, it is apparent that Cu powders are very prone to forming flakes at higher milling energy and these powders are not suitable for most AM processes. However, milling time does not appear to lead to the formation of high aspect ratio flakes and as such provides a processing window for milling powders for AM. Granted low energy conditions are used, high milling times are appropriate for milling even softer metallic powders for prolonged times when mixing different metal feedstock distribution or mixing composite powders.

3.2. Microhardness evolution

Milling *via* HEBM increased microhardness in both SS and Cu powders as shown in Figures 8–10. In Figure 8(a), hardness of SS powders increased from 283 HV (as received) up to 522 HV after 60 min (30 cycles) at a high energy milling condition (BPR of 2:1). In Figure 8(b), processing increased hardness in Cu powders from 53 HV up to 95 HV for powders milled under the high energy condition (BPR 2:1) for 60 min (30 cycles). In the steel powders, it can be seen that hardness increases substantially (413 HV) even in the low energy milling condition with BPR 1:10. Significant hardening occurs even while deformation of the metallic powder was minimal as evidenced by micrographs in Figure 3. Hardening continues steadily as milling transitions to higher energy regimes with BPRs of 1:1 and 2:1. In contrast, Cu powders undergo minimal hardening at low energy regimes, from BPRs of 1:10–1:5. Hardening of Cu powders occurs at higher energy milling conditions with BPR of 1:1, where hardening appears to plateau as nearly identical values (including a wide spread of values) is seen at BPR of 2:1.

In order to delve deeper into the effects of HEBM on hardening of Cu and SS powders, Figures 9 and 10 present hardening over time for both low energy and high energy milling conditions. At a lower energy milling condition (BPR 1:10) steel undergo goes modest hardening initial that then steadily rises. Sixty minutes of milling with BPR of 1:10 results in a 41% increase in hardness. Using the higher energy milling condition (BPR 2:1) results in a rapid rise in hardness, after only 4 min, the hardness exceeds that achieved in the lower energy milling condition after 60 min. Hardness stabilizes at around 20 min, and after 60 min the hardness has increased by 84%, relative to as-received powder. Cu powder behaves substantially different at both low and high energy milling conditions. At low energy condition (BPR 1:10) hardness does not change over time. In the higher energy milling condition (BPR 2:1) hardness does not change significantly until 60 min of milling have elapsed, at which time an increase in hardness of 77% resulted, albeit with a large scatter in values. Interestingly, despite evidence of significant deformation of Cu powders in the high energy milling condition (Figure 6) after 20 min, hardness hardly changes.

Table 1. Aspect ratio and microhardness data for HEBM processed SS and Cu powders.

Sample	BPR	Cycles	Major axis (μm)	Minor axis (μm)	Aspect ratio	Microhardness (HV)
SS-As-received			33.1 ± 17.1	23.1 ± 12.8	1.4 ± 0.8	283 ± 45
SS-2:1-1	2:1	1	10.3 ± 11.0	7.1 ± 8.5	1.5 ± 0.9	326 ± 76
SS-2:1-2	2:1	2	12.1 ± 9.7	8.4 ± 7.4	1.4 ± 0.5	441 ± 137
SS-2:1-5	2:1	5	15.0 ± 14.0	9.3 ± 10.2	1.6 ± 1.5	480 ± 114
SS-2:1-10	2:1	10	23.4 ± 24.6	13.4 ± 15.0	1.7 ± 1.0	516 ± 58
SS-2:1-30	2:1	30	38.3 ± 36.0	20.3 ± 16.8	1.9 ± 0.8	523 ± 69
SS-1:1-1	1:1	1	20.3 ± 12.2	15.1 ± 8.5	1.3 ± 0.4	
SS-1:1-2	1:1	2	21.8 ± 15.6	15.6 ± 10.9	1.4 ± 0.4	
SS-1:1-5	1:1	5	26.2 ± 23.1	16.8 ± 12.8	1.6 ± 0.7	
SS-1:1-10	1:1	10	14.8 ± 17.4	8.8 ± 12.5	1.7 ± 1.2	
SS-1:1-30	1:1	30	8.0 ± 6.6	4.4 ± 4.0	1.8 ± 0.8	489 ± 59
SS-1:5-1	1:5	1	20.0 ± 14.0	12.8 ± 9.0	1.6 ± 0.5	
SS-1:5-2	1:5	2	13.7 ± 9.2	7.9 ± 5.4	1.7 ± 0.4	
SS-1:5-5	1:5	5	20.0 ± 12.0	12.2 ± 8.0	1.6 ± 0.5	
SS-1:5-10	1:5	10	12.3 ± 9.3	8.0 ± 7.0	1.5 ± 0.7	
SS-1:5-30	1:5	30	11.7 ± 11.6	6.8 ± 7.5	1.7 ± 1.2	386 ± 81
SS-1:10-1	1:10	1	9.8 ± 10.1	6.0 ± 7.0	1.6 ± 0.6	258 ± 38
SS-1:10-2	1:10	2	7.7 ± 5.9	4.1 ± 3.2	1.9 ± 0.5	370 ± 77
SS-1:10-5	1:10	5	4.5 ± 2.1	3.4 ± 1.5	1.3 ± 0.4	322 ± 67
SS-1:10-10	1:10	10	12.8 ± 10.3	8.9 ± 7.6	1.4 ± 0.4	323 ± 68
SS-1:10-30	1:10	30	12.9 ± 13.9	7.8 ± 8.5	1.7 ± 0.7	400 ± 61
Cu-As-Received			10.2 ± 8.5	6.1 ± 4.2	1.7 ± 0.6	53 ± 9
Cu-2:1-1	2:1	1	9.8 ± 6.9	6.3 ± 4.8	1.6 ± 0.5	71 ± 27
Cu −2:1-2	2:1	2	10.6 ± 9.9	5.3 ± 4.7	2.0 ± 1.1	71 ± 27
Cu −2:1-5	2:1	5	10.8 ± 7.3	6.2 ± 4.7	1.7 ± 1.0	70 ± 17
Cu −2:1-10	2:1	10	13.9 ± 12.1	6.5 ± 6.2	2.1 ± 1.3	60 ± 12
Cu −2:1-30	2:1	30	16.1 ± 17.1	7.3 ± 10.1	2.2 ± 1.8	95 ± 46
Cu −1:1-1	1:1	1	10.5 ± 6.9	6.3 ± 3.9	1.7 ± 0.7	
Cu −1:1-2	1:1	2	10.6 ± 7.1	5.8 ± 4.2	1.8 ± 0.7	
Cu −1:1-5	1:1	5	11.2 ± 6.9	6.2 ± 4.0	1.8 ± 1.1	
Cu −1:1-10	1:1	10	11.2 ± 8.7	4.8 ± 3.7	2.4 ± 1.5	
Cu −1:1-30	1:1	30	12.0 ± 12.0	6.2 ± 6.2	1.9 ± 1.2	95 ± 48
Cu −1:5-1	1:5	1	10.4 ± 8.1	6.1 ± 4.5	1.7 ± 0.7	
Cu −1:5-2	1:5	2	9.6 ± 6.3	5.5 ± 3.5	1.7 ± 0.7	
Cu −1:5-5	1:5	5	8.8 ± 5.2	5.5 ± 3.3	1.6 ± 0.7	
Cu −1:5-10	1:5	10	10.0 ± 7.9	5.8 ± 4.3	1.7 ± 0.9	
Cu −1:5-30	1:5	30	8.9 ± 5.3	5.1 ± 3.1	1.8 ± 0.7	62 ± 14
Cu −1:10-1	1:10	1	9.5 ± 6.0	5.5 ± 3.2	1.7 ± 0.7	56 ± 16
Cu −1:10-2	1:10	2	9.6 ± 6.6	5.7 ± 4.0	1.7 ± 0.5	51 ± 18
Cu −1:10-5	1:10	5	9.5 ± 6.4	5.8 ± 4.1	1.6 ± 0.5	59 ± 11
Cu-1:10-10	1:10	10	9.3 ± 7.6	5.7 ± 4.6	1.6 ± 0.5	59 ± 14
Cu-1:10-30	1:10	30	7.4 ± 4.7	4.2 ± 2.5	1.8 ± 0.6	52 ± 5

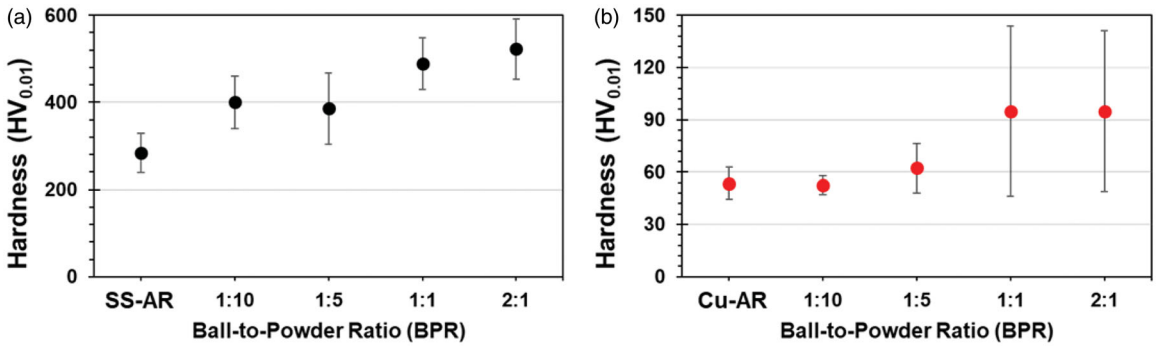

Figure 8. (a) Microhardness of milled 316L stainless steel processed at different BPRs for 60 min (30 cycles) of HEBM, b) Microhardness of milled copper powders processed at different BPRs for 60 min (30 cycles) of HEBM.

These results would at first glance appear paradoxical or perhaps not intuitive. The soft copper material subjected to milling with the harder steel vial and steel balls undergo greater deformation, as evidenced by flakes seen in SEM micrographs (Figure 6), yet hardening occurs to a lesser degree at higher energy milling conditions and is essentially unchanged in the lower energy condition. In contrast, the harder steel undergoes significant hardening even in the lower energy condition. This can be explained by the propensity for a material to harden under deformation, which is quantified by the strain hardening exponent "n" in the relationships between applied strain and strength in Equation (1), where σ is the true stress, ε is the true plastic strain, and K_1 is the strain hardening coefficient.

$$\sigma = K_1 \varepsilon^{n_1} \tag{1}$$

In addition, for face-centered cubic (FCC) materials such as copper and austenitic stainless steels (e.g., 316L stainless

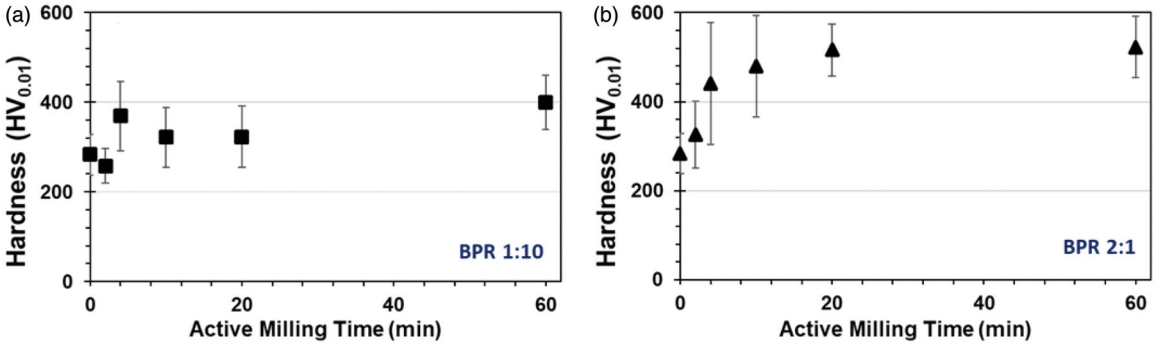

Figure 9. (a) Microhardness of milled 316L stainless steel powders milled for various milling times with either (a) low energy conditions with BPR of 1:10, or (b) high energy conditions with BPR of 2:1.

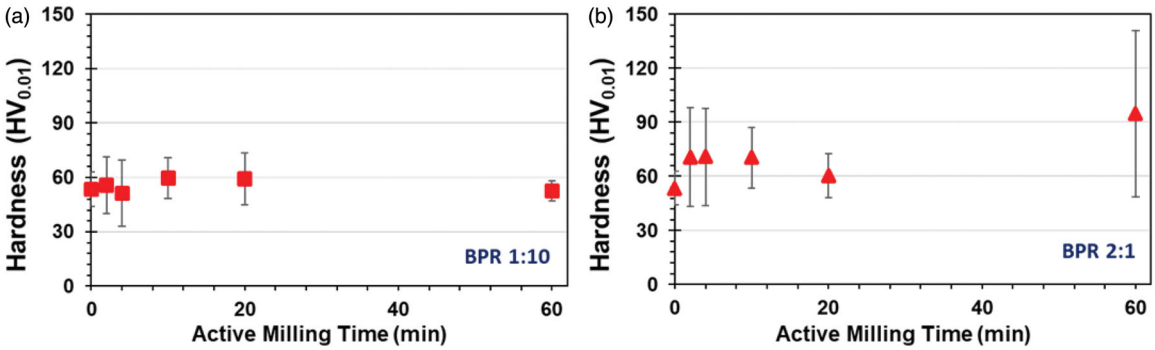

Figure 10. (a) Microhardness of milled copper powders milled for various milling times with either (a) low energy conditions with BPR of 1:10, or (b) high energy conditions with BPR of 2:1.

steel used in this study), additional factors in Equation (2) (constants K_2 and n_2) take into account a larger stress deviation at low strains.

$$\sigma = K_1\varepsilon^{(n_1)} + \exp(K_2 + n_2\varepsilon). \quad (2)$$

These relationships indicate that materials with a higher strain hardening exponent will undergo greater strain hardening (e.g., strengthening) than materials with a lower strain hardening exponent for a given deformation. Cu has a strain hardening exponent ranging from $n\sim0.3-0.32$ in an annealed condition (Lu et al. 2000; Fattah-alhosseini et al. 2016), to as low as ~0.045 in a 25% pre-strained Cu specimen (Fattah-alhosseini et al. 2016). 316L stainless steel has a significantly higher strain hardening exponent of $n\sim0.40$–0.48 at room temperature to ~0.5 at elevated temperature (350 °C) (Samuel and Choudhary 2010; Pintaude, Hoechele, and Cipriano 2012), temperatures not atypical for HEBM processing. Hence, it is seen that the higher strain-hardening exponent of 316L steel makes it more prone to undergoing strain hardening and hence higher hardness for a given amount of deformation induced by the HEBM process. The lower strain hardening exponent of Cu allows it to be severely deformed, as evidenced by the formation of Cu flakes, with minimal increases in hardness initially. Lower, but comparable hardening to 316L SS occurs after 60 min of milling at the higher energy condition.

4. Conclusion

HEBM is an excellent method for processing metallic powders for AM and this study has provided a parameter space for which HEBM can be used to process particulates without significant loss of spheroidicity. Powder morphology is seen to be more sensitive to BPR, with low BPR of 1:10 (low-energy milling) yielding minimal changes, and a higher BPR of 2:1 (intermediate energy milling) yielding flattening of the metallic particulates. Significant flattening leads to a transition from spherical powder to flakes in the softer Cu metal. Flakes are undesirable for many AM applications, including cold spray and SLM, because the high surface area leads to poor flowability. Poor flowability in turn reduces deposition efficiency in cold spray and leads to discontinuous powder beds in SLM. Milling times ranging from 2 to 60 min have less effects on powder morphology at lower energy milling conditions, as observed by SEM and quantified by image analysis. The ability to mill powders for long periods of time is critical to developing composites or mixtures of materials for AM as long milling times increase homogeneity. These results indicate milling times of 60 min can generally be used without affecting spherical morphology. Hardening of the powders was likewise more dependent on BPR than milling time. Hardness increased with increasing BPR for both copper and steel powders. However, 316L stainless steel powders were much more prone to hardening over time even at low BPRs due to the higher strain-hardening exponent, in comparison to Cu. Powder hardening is an important parameter for cold spray where the deposition of the metallic powders is dependent on softening of the particulates and severe deformation upon impact with the substrate. The parameter space described can serve as the foundation for powder processing of alloyed or composite powders for metal AM applications.

Acknowledgments

The authors would like to acknowledge the Hartnell College and California State University at Monterey Bay for supporting and organizing the Hartnell Community College Catalyst (3C) programs that enabled T. Hanneman and A. Gonzalez-Perez to conduct research at NPS during the summer of 2019. We also acknowledge support from the NPS Foundation SEED program and from NPS through the Research Initiation Program.

ORCID

Troy Y. Ansell http://orcid.org/0000-0002-0595-3578
Andy Nieto http://orcid.org/0000-0002-9849-2802

References

Ayoman, E., and S. Ghorban Hosseini. 2016. Synthesis of CuO nanopowders by high-energy ball milling method and investigation of their catalytic activity on thermal decomposition of ammonium perchlorate particles. *Journal of Thermal Analysis and Calorimetry* 123 (2):1213–24. doi:10.1007/s10973-015-5059-1.

Boytsov, O., A. I. Ustinov, E. Gaffet, and F. Bernard. 2007. Correlation between milling parameters and microstructure characteristics of nanocrystalline copper powder prepared via a high energy planetary ball mill. *Journal of Alloys and Compounds* 432 (1–2):103–10. doi:10.1016/j.jallcom.2006.05.101.

Chen, T., J. M. Hampikian, and N. N. Thadhani. 1999. Synthesis and characterization of mechanically alloyed and shock-consolidated nanocrystalline NiAl intermetallic. *Acta Materialia* 47 (8):2567–79. doi:10.1016/S1359-6454(99)00059-2.

Enayati, M. H., M. R. Bafandeh, and S. Nosohian. 2007. Ball milling of stainless steel scrap chips to produce nanocrystalline powder. *Journal of Materials Science* 42 (8):2844–8. doi:10.1007/s10853-006-1371-2.

Fattah-Alhosseini, A., O. Imantalab, Y. Mazaheri, and M. K. Keshavarz. 2016. Microstructural evolution, mechanical properties, and strain hardening behavior of ultrafine grained commercial pure copper during the accumulative roll bonding process. *Materials Science and Engineering: A* 650:8–14. doi:10.1016/j.msea.2015.10.043.

Frazier, W. E. 2014. Metal additive manufacturing: A review. *Journal of Materials Engineering and Performance* 23 (6):1917–28. doi:10.1007/s11665-014-0958-z.

Ghasdi, M., and H. Alamdari. 2010. CO sensitive nanocrystalline $LaCoO_3$ perovskite sensor prepared by high energy ball milling. *Sensors and Actuators B: Chemical* 148 (2):478–85. doi:10.1016/j.snb.2010.05.056.

Gilman, P. S., and J. S. Benjamin. 1983. Mechanical alloying. *Annual Review of Materials Science* 13 (1):279–300. doi:10.1146/annurev.ms.13.080183.001431.

Kaftelen, H., and M. L. Öveçoğlu. 2012. Microstructural characterization and wear properties of ultra-dispersed nanodiamond (UDD) reinforced Al matrix composites fabricated by ball-milling and sintering. *Journal of Composite Materials* 46 (13):1521–34. doi:10.1177/0021998311421636.

Kong, L. B., W. Zhu, and O. K. Tan. 2000. Preparation and characterization of $Pb(Zr_{0.52}Ti_{0.48})O_3$ ceramics from high-energy ball milling powders. *Materials Letters* 42 (4):232–9. doi:10.1016/S0167-577X(99)00190-1.

Li, W., K. Yang, S. Yin, X. Yang, Y. Xu, and R. Lupoi. 2018. Solid-state additive manufacturing and repairing by cold spraying: A review. *Journal of Materials Science & Technology* 34 (3):440–57. doi:10.1016/j.jmst.2017.09.015.

Lu, L., L. B. Wang, B. Z. Ding, and K. Lu. 2000. High-tensile ductility in nanocrystalline copper. *Journal of Materials Research* 15 (2):270–3. doi:10.1557/JMR.2000.0043.

Pintaude, G., A. R. Hoechele, and G. L. Cipriano. 2012. Relation between strain hardening exponent of metals and residual profiles of deep spherical indentation. *Materials Science and Technology* 28 (9–10):1051–4. doi:10.1179/1743284711Y.0000000107.

Raoelison, R. N., Y. Xie, T. Sapanathan, M. P. Planche, R. Kromer, S. Costil, and C. Langlade. 2018. Cold gas dynamic spray technology: A comprehensive review of processing conditions for various technological developments till to date. *Additive Manufacturing* 19:134–59. doi:10.1016/j.addma.2017.07.001.

Samuel, E. I., and B. K. Choudhary. 2010. Universal scaling of work hardening parameters in type 316L(N) stainless steel. *Materials Science and Engineering: A* 527 (27–28):7457–60. doi:10.1016/j.msea.2010.08.021.

Spierings, A. B., M. Voegtlin, T. Bauer, and K. Wegener. 2016. Powder flowability characterisation methodology for powder-bed-based metal additive manufacturing. *Progress in Additive Manufacturing* 1 (1–2):9–20. doi:10.1007/s40964-015-0001-4.

Suryanarayana, C. 2001. Mechanical alloying and milling. *Progress in Materials Science* 46 (1–2):1–184. doi:10.1016/S0079-6425(99)00010-9.

Trudeau, M. L., R. Schulz, D. Dussault, and A. Van Neste. 1990. Structural changes during high-energy ball milling of iron-based amorphous alloys: Is high-energy ball milling equivalent to a thermal process? *Physical Review Letters* 64 (1):99–102. doi:10.1103/PhysRevLett.64.99.

Witkin, D. B., and E. J. Lavernia. 2006. Synthesis and mechanical behavior of nanostructured materials via cryomilling. *Progress in Materials Science* 51 (1):1–60. doi:10.1016/j.pmatsci.2005.04.004.

Wolski, K., G. Le Caër, P. Delcroix, R. Fillit, F. Thévenot, and J. Le Coze. 1996. Influence of milling conditions on the FeAl intermetallic formation by mechanical alloying. *Materials Science and Engineering: A* 207 (1):97–104. doi:10.1016/0921-5093(96)80006-2.

Woo, D. J., B. Sneed, F. Peerally, F. C. Heer, L. C. Brewer, J. P. Hooper, and S. Osswald. 2013. Synthesis of nanodiamond-reinforced aluminum metal composite powders and coatings using high-energy ball milling and cold spray. *Carbon* 63:404–15. doi:10.1016/j.carbon.2013.07.001.

Zheng, R., Z. Zhang, M. Nakatani, M. Ota, X. Chen, C. Ma, and K. Ameyama. 2016. Enhanced ductility in harmonic structure designed SUS316L produced by high energy ball milling and hot isostatic sintering. *Materials Science and Engineering: A* 674:212–20. doi:10.1016/j.msea.2016.07.048.

Zuhailawati, H., H. M. Salihin, and Y. Mahani. 2010. Microstructure and properties of copper composite containing in situ NbC reinforcement: Effects of milling speed. *Journal of Alloys and Compounds* 489 (2):369–74. doi:10.1016/j.jallcom.2009.09.083.